

# Insulating Foams and Dense Geopolymers from Biochar By-Products

R. Farges<sup>1</sup>, A. Gharzouni<sup>1</sup>, B. Ravier<sup>2</sup>, P. Jeulin<sup>2</sup>, S. Rossignol<sup>\*1</sup>

<sup>1</sup>Univ. Limoges, CNRS, IRCER, UMR7315, F-87000 Limoges, France

<sup>2</sup>Etablissement MAILLOT, F-28500 Vernouillet, France

received December 22, 2017; received in revised form February 28, 2018; accepted March 12, 2018

## Abstract

Pyrolysis is an innovative environmentally-friendly process to thermally treat biomass residues at low temperatures and in the absence of oxygen without releasing suspended particles, smoke or greenhouse gases. The obtained solid residue is called biochar. The aim of this work is to characterize four biochar by-products and to evaluate the feasibility of biochar-based geopolymer materials. For this, four types of biochar by-products, produced from wheat straw, miscanthus and wood, under different pyrolysis conditions were studied. First, the physical and chemical properties of the biochar by-products were determined. Structural data were obtained with infrared spectroscopy (FTIR) and X-ray diffraction. Then a feasibility study of consolidated materials and foams was initiated. The results show that the biochar by-product is essentially chemically composed of silicon, potassium and calcium. Differences are observed depending on the type of biomass used to obtain the biochar by-product. Geopolymer binders were successfully synthesized from biochar by-products and a metakaolin. Furthermore, biochar by-product-based geopolymer foams were obtained using silica fume without metakaolin. The obtained materials exhibit low thermal conductivity values ( $\approx 0.13$  W/mK), which suggests their use for insulation applications.

*Keywords:* Biochar, FTIR, geopolymer, foams, thermal conductivity

## I. Introduction

Biochar is a solid product formed after the pyrolysis (thermal decomposition) of biomass residues, lignocellulosic feedstocks or organic wastes at low temperatures and in the absence of oxygen. Consequently, the term “biochar” includes a large range of residues which essentially depend on the biomass starting materials (chemical composition, particle size) and on the pyrolysis process conditions (temperature, duration, atmosphere)<sup>1</sup>. The biomass starting materials contain essentially cellulose, hemicellulose and lignin in different proportions. These components decompose at different temperatures, consequently influencing the physical, chemical and structural characteristics of the resulting biochar<sup>2</sup>. Biochar is generally considered as a cost-effective, sustainable and ecofriendly material because it originates from waste and does not need any addition of chemical reagents<sup>3</sup>. Moreover, biochar properties can be improved with additional thermal, chemical or physical treatment. For example, activated biochars are characterized by their higher specific surface, which improves their sorptive properties<sup>4</sup>. Many biochar applications can be considered. Given that biochar contains a high content of carbon, it can be used as fuel for generating energy<sup>5</sup>. Moreover, biochar has been used in sorption, stabilization and environmental protection and remediation owing to its ability to reduce the mobility of pollutants and organic compounds<sup>6-8</sup>. Until now, the main use of biochar has been in agriculture as soil amend-

ment because it has been demonstrated that it improves the biological and physical properties of the soil, which enhances fertility and crop production<sup>9-10</sup>.

A promising and innovative alternative is the use of biochar to produce geopolymer materials. Geopolymer materials are low-energy-consuming and eco-friendly mineral binders. These materials can be defined as amorphous aluminosilicate binders synthesized by the activation of an aluminosilicate source by an alkaline solution at atmospheric pressure and a temperature below 100 °C<sup>11</sup>. Geopolymers show high mechanical properties and good durability when exposed to chloride or sulphate attack. Moreover, geopolymer foams can be realized by adding a foaming agent to the reactive mixture such as silica fume<sup>12-13</sup>, aluminium powder or hydrogen peroxide<sup>14</sup>.

This work focuses on the characterization of physico-chemical and structural properties of four biochar by-products. Then a feasibility study of biochar-based geopolymers and foams was evaluated.

## II. Material and Methods

### (1) *Materials*

#### (a) *Raw materials preparation*

Three types of biomass were supplied by agricultural cooperatives (wheat straw, miscanthus and short rotation coppice (SRC)). They were treated independently by means of pyrolysis at different temperatures without milling, using the Biolyse® process in order to obtain a

\* Corresponding author: [sylvie.rossignol@unilim.fr](mailto:sylvie.rossignol@unilim.fr)

solid residue called biochar by-product. These materials are supplied by Maillot and denoted  $M_{WS1}$ ,  $M_{WS2}$ ,  $M_M$  and  $M_{SRC}$  as reported in Table 1. Then, they were milled in a planetary grinder for five minutes. A part of these biochar by-products was calcined for 1 h at 500 °C with heating rates of 5 K/min to 250 °C and 1 K/min from 250 °C to 500 °C. These calcined materials are indicated with the sign (\*).

### (b) Sample preparation

Samples were prepared using a commercial potassium silicate solution supplied by Woellner and denoted S1 with a Si/K molar ratio equal to 1.75<sup>15</sup>. A metakaolin supplied by Imerys denoted M1 and four biochar by-products denoted  $M_{WS1}$ ,  $M_{WS2}$ ,  $M_M$  and  $M_{SRC}$  were used as aluminosilicate sources. Potassium hydroxide pellets (KOH, 85.2 % pure) were dissolved into potassium silicate solution in order to obtain a Si/K molar ratio equal to 0.54. Then, metakaolin or biochar by-products were added. In order to obtain foams, silica fume is used as foaming agent during mixing<sup>16</sup> with an alkaline solution with a Si/K molar ratio equal to 0.67 and without metakaolin. Samples were placed in closed square PTFE moulds and stored in an air oven at 40 °C for 24 h. Different conditions were applied to the foams: drying at 40 or 90 °C in an oven in air, storage in the lab ( $T = 20$  °C; RH = 45 %) or in a moist environment ( $T = 20$  °C; RH = 85 %).

Potassium alkaline solution has been used in this study owing to its higher reactivity and lower viscosity compared to sodium alkaline solution. Indeed, according to the literature, potassium-based geopolymer exhibits higher compressive strength than sodium-based geopolymer<sup>17</sup>. Moreover, a low Si/K molar ratio of the alkaline solution varying between 0.5 and 1.0 was proven with Raman and NMR spectroscopies to induce higher reactivity owing to a higher depolymerization degree<sup>15,18</sup>. In fact, when the Si/K ratio decreases, the higher amount of depolymerized species enhances the polycondensation reaction, leading to better mechanical properties of the final geopolymers.

### (2) Characterizations

The chemical composition of calcined biochar by-products was determined using X-ray fluorescence (Zetium spectrometer, PANalytical). The particle size distributions of the biochar by-products were measured using a laser particle size analyzer (Mastersizer 2000). The measurement was performed in dry conditions at a pressure of 2 or 3 bar depending on the powder.

X-ray diffraction patterns were acquired in X-ray diffraction (XRD) experiments on a D8 Bruker Advance powder diffractometer using  $\text{CuK}\alpha$  ( $\lambda_{\text{K}\alpha} = 0.154186$  nm). The analytical range is between 5° and 50° (2 $\theta$ ) with a step of 0.015° and a step time of 576 s. ICDD (International Centre for Diffraction Data) files were used for phase identification.

FTIR spectra were obtained on a ThermoFisher Scientific 380 infrared spectrometer (Nicolet). Transmission mode was used on KBr pellets containing 1 mg raw or calcined biochar by-products. Acquisitions were realized over a range of 400 to 4000  $\text{cm}^{-1}$  with a resolution of 4  $\text{cm}^{-1}$ . The atmospheric  $\text{CO}_2$  contribution present between 2280 and 2400  $\text{cm}^{-1}$  was removed via a straight-line fit. To enable comparison, the spectra were baseline corrected and normalized.

The density of the biochar by-products was determined with the pycnometer method.

Differential thermal analysis (DTA) and thermogravimetric analysis (TGA) of raw biochar by-products were performed on an SDT Q600 apparatus from TA Instruments in an atmosphere of flowing dry air (100 mL/min) in alumina crucibles. The analysis was performed from 30 to 600 °C at 5 K/min.

The thermal conductivity was measured using a hot-disk thermal analyser (TPS 1500, Hot disk) at room temperature. The foams were cut into two parts with a ribbon saw. The measuring time, the radius of the disk sensor and the output power used were 80 seconds, 6.394 mm and 0.052 W, respectively.

The compressive strengths were determined using a LLOYD EZ20 universal testing machine with a strength sensor of 20 kN and a crosshead speed of 0.5 mm/min. The compressive tests were performed on six samples for each composition. The samples were cylindrical in shape with a diameter of 15 mm and a height of approximately 30 mm. They were aged for seven days in a closed mould at room temperature ( $T = 20$  °C).

## III. Results and Discussion

### 3.1. Biochar by-products study

#### (a) Physicochemical characteristics

The physicochemical characteristics are detailed in Table 1. The four biochar by-products were obtained from the pyrolysis of three different types of biomass

**Table 1:** Chemical and physical characteristics of biochar by-products.

Nomenclature	Types of biomass	Pyrolysis temperature (°C)	$d_{50}$ ( $\pm 1$ $\mu\text{m}$ )	Density ( $\pm 0.01$ $\text{g}/\text{cm}^3$ )	Carbon content ( $\pm 1$ %)
$M_{WS1}$	Wheat straw	159	19	1.44	88
$M_{WS2}$	Wheat straw	360	21	1.57	79
$M_M$	Miscanthus	272	20	1.46	93
$M_{SRC}$	SRC	405	27	1.57	88

at different temperatures:  $M_{WS1}$  (wheat straw /159 °C),  $M_{WS2}$  (wheat straw /360 °C),  $M_M$  (Miscanthus /272 °C) and  $M_{SRC}$  (SRC /405 °C). Concerning  $M_{WS1}$  and  $M_{WS2}$ , based on the same biomass, the median diameter is equal to 19 and 21  $\mu\text{m}$  for  $M_{WS1}$  and  $M_{WS2}$  respectively. It can be explained by the higher pyrolysis temperature of  $M_{WS2}$ , which leads to particle densification and the evacuation of the organic compounds<sup>19</sup>. This result is in agreement with the density values equal to 1.44 and 1.57  $\mu\text{m}$  for  $M_{WS1}$  and  $M_{WS2}$ , respectively. Furthermore, the carbon contents of  $M_{WS1}$  and  $M_{WS2}$  are equal to 88 and 79 wt%. This difference is also due to the pyrolysis temperature<sup>20</sup>. For the other samples, the median diameter of particles of  $M_{WS2}$ ,  $M_M$  and  $M_{SRC}$  are globally similar (21, 20 and 27  $\mu\text{m}$ , respectively). Density values are equal to 1.46, 1.57, 1.57  $\text{g}/\text{cm}^3$  for  $M_M$ ,  $M_{WS2}$  and  $M_{SRC}$ , respectively. Furthermore, the carbon content of  $M_{WS2}$ ,  $M_{SRC}$  and  $M_M$  is equal to 79, 88 and 93 wt%, respectively. The higher pyrolysis temperature involves a particular densification and a decrease in carbon content, but the nature of the biomass induces differences with regard to chemical composition. Furthermore, all these materials exhibit hydrophobic behaviour, which can be explained based on the high carbon content<sup>21</sup>.

The chemical compositions presented in Table 2 show that calcined biochar by-products are mainly composed of silicon, potassium, calcium, chlorine, sulphur and phos-

phor. The results for  $M_{WS1}^*$  and  $M_{WS2}^*$ , biochar by-products obtained from wheat straw at different temperatures, are globally similar. The K/Si and Ca/Si molar ratio are about 0.28 and 0.09, respectively. The S/Si, P/Si, Mg/Si and Al/Si molar ratio are equal except the Fe/Si molar ratio which is higher for  $M_{WS2}^*$  (0.09). This difference can be due to the temperature of the process. Molar ratios of  $M_M^*$  are globally similar to  $M_{WS2}^*$  except the P/Si molar ratio which is higher for  $M_M^*$  (0.09). This result can be explained by the nature of the biomass, which can induce differences in the chemical composition. Concerning  $M_{SRC}^*$ , the K/Si, Ca/Si, P/Si and Mg/Si molar ratios are higher than that of the other biochar by-products. This fact can be explained by the difference in terms of chemical composition of the SRC biomass (wood) compared to miscanthus and wheat straw.

In summary, the physicochemical characteristics of the four biochar by-products highlight some differences concerning the amorphous structure content, especially for  $M_{SRC}$ , which suggests different reactivity in alkaline media.

#### (b) Thermal analysis

Thermal analysis curves (DTA and TGA), reported in Fig. 1, show exothermic peaks linked to weight losses centred at around 290, 380 and 425 °C. For  $M_{WS1}$  and  $M_{WS2}$  samples, the first exothermic peak, attributed to

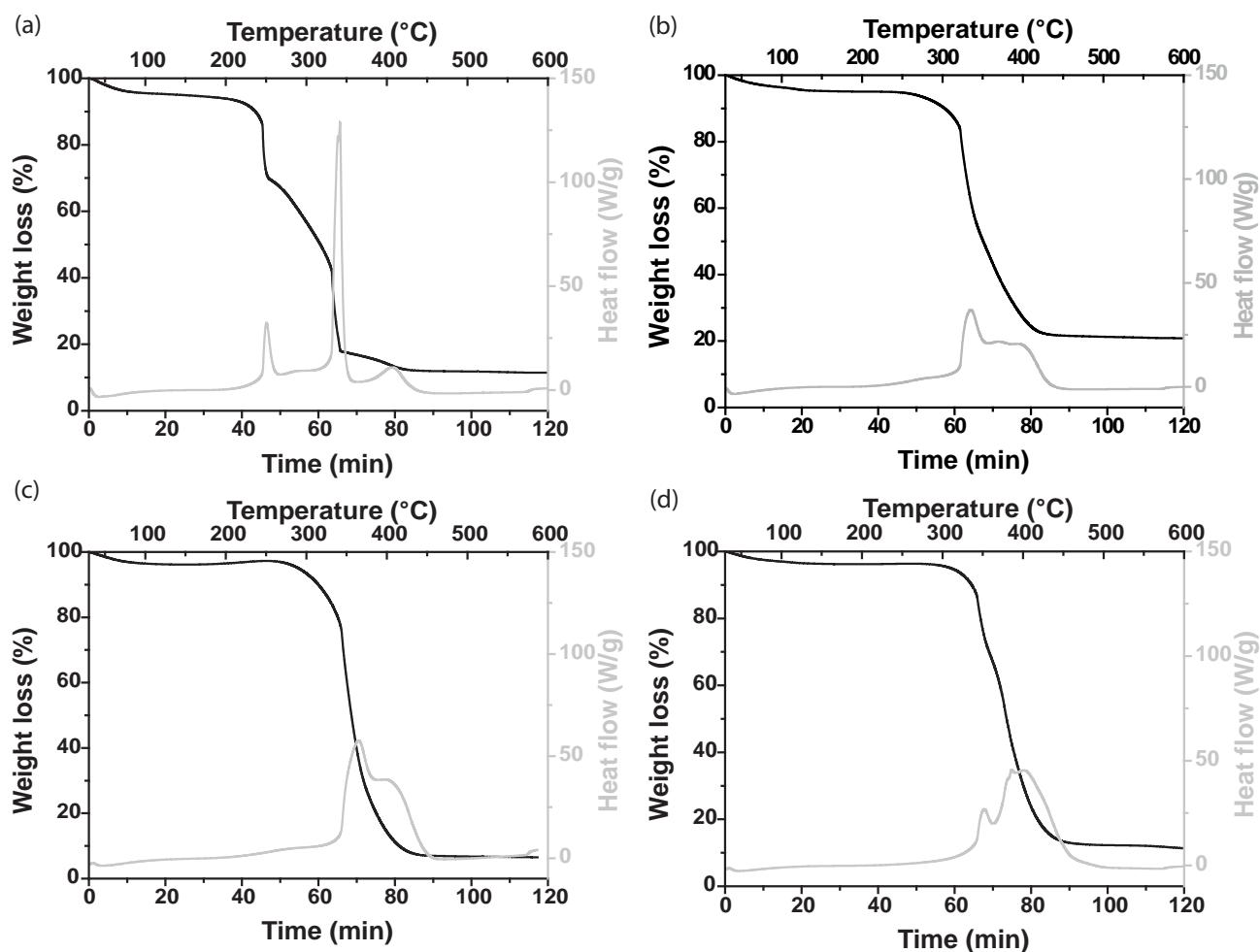


Fig. 1: DTA and TGA curves of (a)  $M_{WS1}$ , (b)  $M_{WS2}$ , (c)  $M_M$  and (d)  $M_{SRC}$  biochar by-products.

**Table 2:** Chemical composition of calcined biochar by-products.

Nomenclature	Carbon analysis (wt%)	Molar ratio						
	C	K/Si	Ca/Si	S/Si	P/Si	Mg/Si	Fe/Si	Al/Si
$M_{WS1}^*$	1.67	0.32	0.10	0.03	0.03	0.03	0.01	0.01
$M_{WS2}^*$	1.27	0.23	0.08	0.03	0.02	0.03	0.09	0.01
$M_M^*$	1.21	0.29	0.07	0.05	0.09	0.05	0.05	0.02
$M_{SRC}^*$	6.82	1.96	3.76	0.44	1.06	0.69	0.07	0.04

the decomposition of hemicellulose occurs at 280 and 291 °C<sup>22–23</sup>. The weight loss associated with this exothermic peak is higher for  $M_{WS1}$  than for  $M_{WS2}$  (32 and 3 % respectively). It shows that hemicellulose is conserved during the pyrolysis process of  $M_{WS1}$ . The second peak, at around 372 °C, is due to cellulose decomposition<sup>23–24</sup>. The weight loss observed for  $M_{WS1}$  and  $M_{WS2}$  is about 45 %, suggesting that the cellulose is not impacted by the pyrolysis temperature. The third peak attributed to lignin decomposition occurs at 424 and 417 °C for  $M_{WS1}$  and  $M_{WS2}$  respectively<sup>23–24</sup>. The weight losses observed for  $M_{WS1}$  and  $M_{WS2}$  are equal to 5 and 25 % respectively. This difference can be explained by the different sampling performed during the collection before the investigations.

The peak attributed to hemicellulose decomposition is not observed for  $M_M$  and  $M_{SRC}$  because of the higher temperature of pyrolysis. On the other hand, the two peaks attributed to cellulose and lignin decomposition are observed.  $M_{WS2}$  contains more cellulose than  $M_M$  and  $M_{SRC}$  considering the weight loss value equal to 46 % at about 385 °C. On the other hand,  $M_M$  and  $M_{SRC}$  contain more lignin than  $M_{WS2}$  (63 and 55 % respectively) considering the weight loss between 385 and 485 °C. The presence of a shoulder suggests the existence of different types of lignocellulosic species.

Thermal treatment at 500 °C is realized on the four biochar by-products in order to reduce the carbon content and to determine the chemical composition by means of X-ray fluorescence. Carbon contents of  $M_{WS1}^*$ ,  $M_{WS2}^*$ ,  $M_M^*$  and  $M_{SRC}^*$ , presented in Table 2, are equal to 1.67, 1.27, 1.21 and 6.82 wt%, respectively. This suggests that short rotation coppice biomass (SRC) contains more lignocellulosic species that are resistant to pyrolysis treatment.

### (c) Structural characteristic

FTIR spectra, presented in Fig. 2A, show differences between the biochar by-products. The infrared spectrum of  $M_{WS1}$  biochar by-product (Fig. 2A-a) highlights the presence of a broad band at 3300 cm<sup>-1</sup> due to O-H stretching vibration<sup>25–26</sup>. Bands at 2900 and 2080 cm<sup>-1</sup> are due to C-H vibration as mentioned by<sup>25, 27</sup>. The band at 1700 cm<sup>-1</sup> is due to C=O stretching of acetyl and ester groups of hemicellulose<sup>28</sup>. The broad band at 1600 cm<sup>-1</sup> is attributed to water–H<sub>2</sub>O. Bands around 1500 cm<sup>-1</sup> are due to C=O and aromatic C=C stretching vibrations<sup>29–30</sup>. Characteristics bands of–CO<sub>3</sub> group of calcite at 1460, 1420, 873 and 712 cm<sup>-1</sup> are note-

worthy<sup>31–32</sup>. Bands present in the range between 1200 and 900 cm<sup>-1</sup> are due to Si-O-Si stretching<sup>33–34</sup>. Moreover, bands at 1170, 1070 and 620 cm<sup>-1</sup> are attributed to symmetric stretching and asymmetric bending respectively of–SO<sub>4</sub><sup>2-</sup> group<sup>35</sup>. Bands at 1111, 980 and 568 cm<sup>-1</sup> are due to antisymmetric stretching, symmetric stretching and antisymmetric bending of (PO<sub>4</sub>)<sup>3-</sup>, respectively<sup>36</sup>. FTIR spectra of calcined biochar by-products at 500 °C (Fig. 2B) show differences compared to the raw materials. The thermal treatment at 500 °C induces the release of water and the decomposition of carbon compounds (lignocellulosic species). Indeed, for the biochar by-products  $M_{WS1}^*$  (Fig. 2B-a) and  $M_{WS2}^*$  (Fig. 2B-b) from wheat straw, bands at 3300, 2900 and 2200 cm<sup>-1</sup> have disappeared. Bands at about 1420, 873 and 712 cm<sup>-1</sup> due to calcite are preserved. Moreover, sulphates bands at 1170 and 620 cm<sup>-1</sup> are preserved too. Bands at 1111, 980 and 568 cm<sup>-1</sup> due to the vibrations of PO<sub>4</sub><sup>3-</sup> and a broad band centred at about 1000 cm<sup>-1</sup> corresponding to Si-O-Si stretching are observed. The two spectra are globally similar given that  $M_{WS1}^*$  and  $M_{WS2}^*$  are obtained from the same wheat straw and the same calcination at 500 °C. The spectrum of  $M_M^*$  (Fig. 2B-c) is quite similar to that of  $M_{WS2}^*$ , which means that wheat straw and miscanthus seem to have similar chemical groups after calcination at 500 °C. The spectrum of  $M_{SRC}^*$  is completely different from the other biochar by-products. Indeed, bands at 1420, 873, 711 and 693 cm<sup>-1</sup> induced by carbonates are very pronounced. The centre of the broad band of Si-O-Si shifts from 1000 to 1036 cm<sup>-1</sup>. These results show that the chemical composition of SRC biomass is different from that of miscanthus and wheat straw.

The infrared spectrum of  $M_{WS2}$  biochar by-product (Fig. 2A-b) is different from the  $M_{WS1}$  spectrum. Bands at 3300 and 2900 cm<sup>-1</sup> attributed to O-H and C-H stretching, respectively, are indeed less pronounced. These results are in agreement with the higher pyrolysis temperature, which is responsible for the decrease in carbon content. It suggests that organic compounds like cellulose are eliminated during the Biolyse® process. Carbonates bands around 1450 cm<sup>-1</sup> are more pronounced and a broader band of Si-O-Si binding centred at 1000 cm<sup>-1</sup> is observed.

Bands observed in the infrared spectrum of  $M_M$  biochar by-product (Fig. 2A-c) are due to the same groups. Some differences exist regarding the intensity of O-H and C-H bands at 3300 and 2900 cm<sup>-1</sup> because of the low pyrolysis temperature.



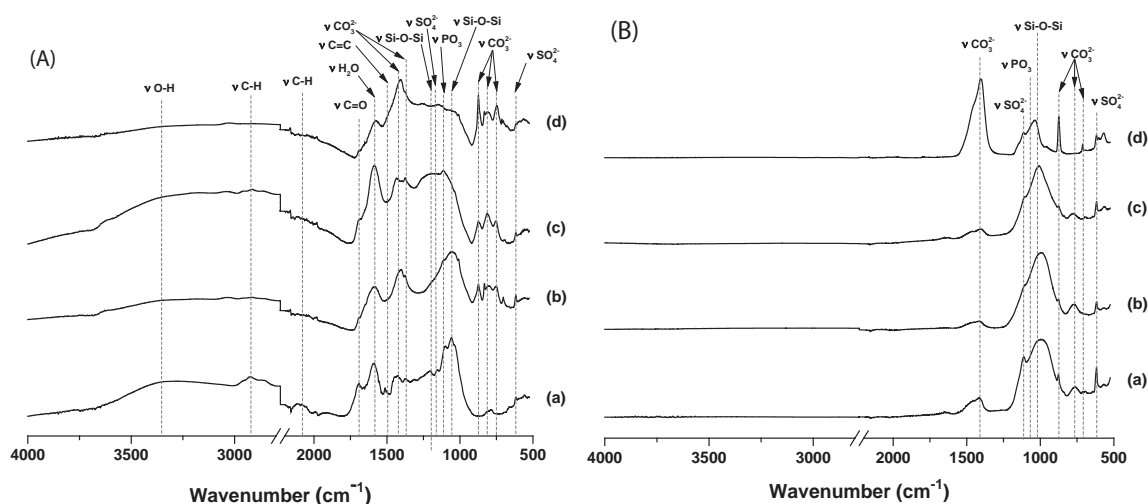


Fig. 2: FTIR spectra of (A) raw and (B) calcined (a)  $M_{WS1}$ , (b)  $M_{WS2}$ , (c)  $M_M$  and (d)  $M_{SRC}$  biochar by-products.

$M_{SRC}$  biochar by-product (Fig. 2A-d) is different from the others. Indeed, bands due to organic compounds are quasi non-existent and carbonate bands are very pronounced. These results are in agreement with the fact that the nature of the biomass is different, leading to variation in chemical composition.

The XRD patterns (Fig. 3A) of all biochar by-products show the presence of peaks relative to crystalline phases and of a broad dome in the  $20-30^\circ$  ( $2\theta$ ) range characteristic of the amorphous structure. This dome is less predominant in  $M_{WS2}$  than in  $M_{WS1}$  and its centre is displaced from  $22^\circ$  to  $24^\circ$  ( $2\theta$ ). This difference is due to the lower carbon content because of the higher pyrolysis temperature. Crystalline phases are similar in  $M_{WS1}$  and  $M_{WS2}$ . Quartz  $SiO_2$ , sylvite  $KCl$ , arcanite  $K_2SO_4$  and potassium phosphate  $K_3PO_4$  are the main minerals. Calcite  $CaCO_3$  is also present, but peaks are more predominant for  $M_{WS2}$  and a peak attributed to  $Ca_2P_2O_7$  is observed in  $M_{WS2}$ . These results are in agreement with the chemical composition obtained with X-ray fluorescence.  $M_{WS2}$ ,  $M_M$  and  $M_{SRC}$  XRD patterns highlight the presence of a broad dome centred at around  $24^\circ$  ( $2\theta$ ) and crystalline phases observed are globally similar. Peaks are less predominant for  $M_M$  than

for the others. The  $M_{SRC}$  XRD pattern shows the presence of fairchildite  $K_2Ca(CO_3)_2$  and peaks relative to calcite are more predominant. Furthermore, the intensity of peaks relative to sylvite is lower.  $M_{SRC}$  has the higher calcium content. XRD patterns of calcined biochar by-products are shown in Fig. 3B. The intensity of the broad dome observed in the  $20-30^\circ$  ( $2\theta$ ) range for the raw materials has decreased. It coincides with the reduction in carbon content. Sylvite ( $KCl$ ), calcite ( $CaCO_3$ ), arcanite ( $K_2SO_4$ ) and quartz ( $SiO_2$ ) are the main crystalline phases observed in  $M_{WS1}^*$  and  $M_{WS2}^*$ . In  $M_M^*$  biochar by-product, the intensity of peaks attributed to  $KCl$  is lower than in  $M_{WS1}^*$  and  $M_{WS2}^*$  and peaks of  $CaCO_3$  are more pronounced. Moreover, peaks attributed to  $K_3PO_4$  and to  $KAl(SO_4)_2$  are observed. Thus, it has been shown that the composition of wheat straw and miscanthus is different. In  $M_{SRC}^*$  biochar by-product, the intensity of the  $KCl$  peaks decreases. Moreover,  $K_3PO_4$  peaks are very pronounced and a new crystalline phase ( $K_2Ca(CO_3)_2$ ) is observed.

Consequently, the four biochar by-products exhibit different mineralogical compositions depending on the parent biomass and the temperature of pyrolysis.

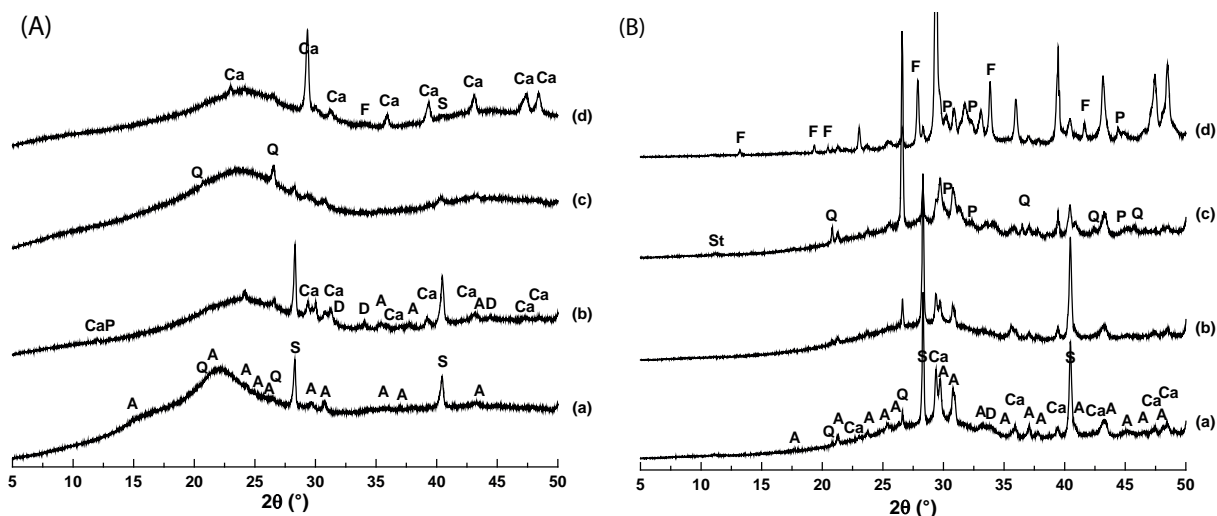


Fig. 3: XRD patterns of (A) raw and (B) calcined (a)  $M_{WS1}$ , (b)  $M_{WS2}$ , (c)  $M_M$  and (d) biochar by-products [ICDD files:  $SiO_2$  (Q) 04-007-5142;  $KCl$  (S) 04-008-1875;  $K_2SO_4$  (A) 00-044-1414;  $CaCO_3$  (Ca) 04-012-8072;  $K_2Ca(CO_3)_2$  (F) 00-021-0981;  $K_3PO_4$  (P) 00-018-1049;  $KAl(SO_4)_2$  (St) 00-047-1883;  $Ca_2P_2O_7$  (CaP) 00-041-0489].

### 3.2. Geopolymer feasibility

#### (a) Dense materials

A feasibility study of consolidated materials with a different amount of biochar by-products was initiated. A known metakaolin-based geopolymer composition was used as a reference. Then, the metakaolin was progressively substituted with the four studied biochar raw materials ( $M_{WS1}$ ,  $M_{WS2}$ ,  $M_M$  and  $M_{SRC}$ ). The results show the possibility to substitute 40 wt% of metakaolin with each biochar by-product. The obtained mixtures are dark, viscous and can be easily cast into moulds with different shapes. After 24 hours, the resulting materials, presented in Table 3, are consolidated and homogeneous with a smooth and shiny aspect. The samples are dark and less dense than conventional geopolymers owing to their carbon content, which lightens the materials. Mechanical properties of the different biochar-based samples were evaluated after seven days in compressive strength tests.  $M_{WS1}$ -based samples were too fragile to undergo surface treatment and their mechanical resistance was estimated at 3 MPa.  $M_{WS2}$ ,  $M_M$  and  $M_{SRC}$  biochar-based samples exhibit similar and higher compressive strength values of 10, 12 and 13 MPa, respectively. The difference between the compressive strength values of the  $M_{WS1}$  biochar-based samples and those of the other samples ( $M_{WS2}$ ,  $M_M$  and  $M_{SRC}$ ) can be explained based on the difference in the pyrolysis temperature of the biomass. A higher pyrolysis temperature of the used biochar induces a higher decomposition of organic compounds (such as hemicellulose) as previously demonstrated with thermal analysis, which leads to higher reactivity in an alkaline solution and better compressive strength values.

Consequently, dense materials based on 60 wt% metakaolin and 40 wt% biochar have been successfully synthesized and exhibit compressive strength of about

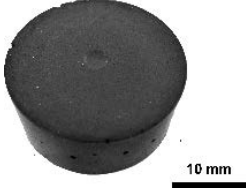
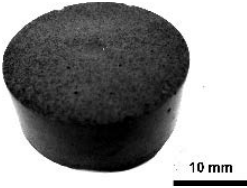

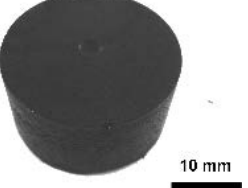
12 MPa. The organic compounds present in the mixture seem to influence the mechanical strength.

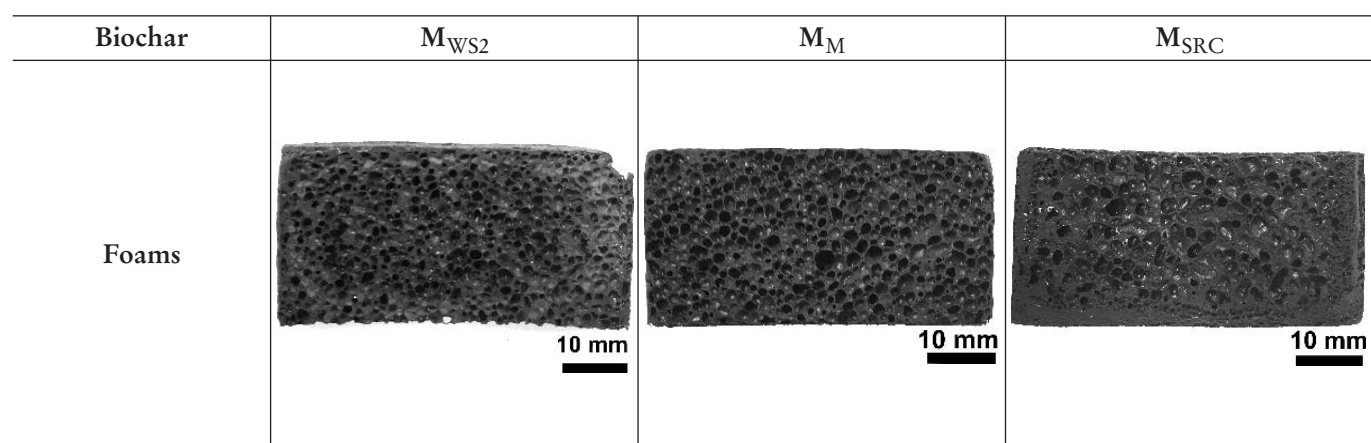
#### (b) Foam materials

Biochar-based foam materials were also obtained using a solution of potassium silicate and a foaming agent (silica fume) without metakaolin (Table 4). Thermal conductivities of obtained foams were measured after different storage and drying conditions (relative humidity and temperature) as listed in Table 5. The results show that after storage for seven days at ambient temperature and relative humidity ( $T = 20^\circ\text{C}$ ;  $\text{RH} = 45\%$ ), thermal conductivity values are equal to 0.20, 0.18 and 0.19 W/mK for  $M_{WS2}$ -,  $M_M$ - and  $M_{SRC}$ -based foams, respectively. Whichever biochar was used, the obtained values are similar and relatively high for insulation applications. Drying at  $90^\circ\text{C}$  enables a reduction in the thermal conductivity to 0.15, 0.14 and 0.14 W/mK for  $M_{WS2}$ -,  $M_M$ - and  $M_{SRC}$ -based foams, respectively. This result shows that the dehydration of water reduces the specific heat and therefore the thermal conductivity, which is in agreement with the work of Duxson *et al.*<sup>37</sup>. After four months of storage ( $T = 20^\circ\text{C}$ ;  $\text{RH} = 45\%$ ), the thermal conductivity of the foams is preserved and equal to 0.15, 0.15 and 0.16 W/mK for  $M_{WS2}$ -,  $M_M$ - and  $M_{SRC}$ -based foams respectively. This fact evidences that thermal properties do not evolve over time. After seven months, the foams were stored in a high relative humidity environment ( $\text{RH} = 85\%$ ) for two days and dried at  $40^\circ\text{C}$ . These conditions do not damage the foams' aspect and do not seem to modify their thermal conductivity values, which highlights a resistance to humidity.

All these data show the possibility to use biochar by-products with silica fume to synthesize foams. The obtained foams present a stability over time with interesting thermal properties (0.13 W/mK).

**Table 3:** Photos and compressive strength of biochar-by-product-based dense geopolymers.

Biochar	$M_{WS1}$	$M_{WS2}$	$M_M$	$M_{SRC}$
Dense geopolymers				
Compressive strength ( $\pm 1$ MPa)	3	10	12	13

**Table 4:** Photos of biochar-by-product-based foams.**Table 5:** Thermal conductivity of biochar-by-products-based foams after different conditions.

Biochar-based foams	Synthesis	Storage (20 °C)	Drying	Thermal conductivity	
	T (°C)	RH (%)	T (°C)	Age (days)	$\lambda$ ( $\pm 0.01$ W/mK)
$M_{WS2}$	40	45	–	7	0.20
		45	90	9	0.15
		45	–	140	0.15
		85	40	205	0.13
$M_M$	40	45	–	7	0.18
		45	90	9	0.14
		45	–	140	0.15
		85	40	205	0.13
$M_{SRC}$	40	45	–	7	0.19
		45	90	9	0.14
		45	–	140	0.16
		85	40	205	0.13

#### IV. Conclusions

A study was initiated to characterize four biochar by-products in order to evaluate their suitability to produce geopolymer materials. The results evidence that physico-chemical and structural characteristics depend on: (i) the nature and the chemical composition of the biomass, and (ii) the pyrolysis temperature. Indeed, different amounts of carbon, silicon, calcium, potassium, sulphur and phosphorus are observed according to the nature of the biomass and suggest different reactivity. Two types of materials have been synthesized: (i) dense materials with the substitution of 40% of metakaolin with biochar by-products and (ii) foams using silica fume without metakaolin with interesting insulation properties (thermal conductivity  $\approx 0.13$  W/mK) and stability over time. To sum up, biochar can be valorised to produce geopolymer materials.

#### References

- Lehmann, J., Joseph, S.: Biochar for environmental management: Science and technology (first ed.), Earthscan. London (UK). 2009.
- Lehmann, J., Joseph, S.: Biochar for environmental management: Science and technology (second ed.), Earthscan. London (UK). 2015.
- Bridgwater, A.V.: Renewable fuels and chemicals by thermal processing of biomass, *Chem. Eng. J.*, **91**, 87–102, (2003).
- Sricharoenchaikul, V., Pechyen, C., Aht-ong, D., Atong, D.: Preparation and characterization of activated carbon from the pyrolysis of physic nut (*Jatropha curcas* L.), *Waste. Energ. Fuel.*, **22**, 31–37, (2008).
- Bridgwater, A.V.: Review of fast pyrolysis of biomass and product upgrading, *Biomass Bioenerg.*, **38**, 68–94, (2012).
- Uchimiya, M., Chang, S., Klasson, K.T.: Screening biochars for heavy metal retention in soil: Role of oxygen functional group, *J. Hazard Mater.*, **190**, 432–441, (2011).
- Verheijen, F., Jeffery Simon, L., Bastos, A.C., Van Der Velde, M., Dias, I.: Biochar application to soils – a critical scientific review of effects on soil properties, processes and functions,

- (EUR - scientific and technical research reports), European Commission. 2010.
- 8 Zhao, X., Wang, J., Wang, S., Xing, G.: Successive straw biochar application as a strategy to sequester carbon and improve fertility: A pot experiment with two rice/wheat rotations in paddy soil, *Plant Soil*, **378**, 279–294, (2014).
  - 9 Lehmann, J., Pereira da Silva, J., Steiner, C., Nehls, T., Zech, W., Glaser, B.: Nutrient availability and leaching in an archaeological anthrosol and a ferralsol of the central amazon basin: fertilizer, manure and charcoal amendments, *Plant Soil*, **249**, 343–357, (2003).
  - 10 Sohi, S.P., Krull, E., Lopez-Capel, E., Bol, R.: A review of biochar and its use and function in soil, *Adv. Agron.*, **105**, 47–82, (2010).
  - 11 Davidovits, J.: Geopolymer: Chemistry and applications, 2nd edition, Institut Geopolymer, St-Quentin (FR). 2008
  - 12 Prud'homme, E., Michaud, P., Joussein, E., Clacens, J-M., Rossignol, S.: Role of alkaline cations and water content on geomaterial foams: monitoring during formation, *J. Non-Cryst. Solids*, **357**, [4], 1270–1278, (2011).
  - 13 Papa, E., Medri, V., Kpogbemabou, D., Morinière, V., Laumonier, J., Vaccari, A., Rossignol, S.: Porosity and insulating properties of silica-fume based foams, *Energ. Buildings*, **131**, 223–232, (2016).
  - 14 Masi, G., Rickard, W.D.A., Vickers, L., Bignozzi, M.C., Van Riessen, A.: A comparison between different foaming methods for the synthesis of light weight geopolymers, *Ceram. Int.*, **40**, 13891–13902, (2014).
  - 15 Gharzouni, A., Joussein, E., Samet, B., Baklouti, S., Rossignol, S.: Effect of the reactivity of alkaline solution and metakaolin on geopolymer formation, *J. Non-Cryst. Solids*, **410**, 127–134, (2015).
  - 16 Prud'homme, E., Michaud, P., Joussein, E., Peyratout, C., Smith, A., Rossignol, S.: *In situ* inorganic foams prepared from various clays at low temperature, *Appl. Clay Sci.*, **51**, 15–22, (2011).
  - 17 Duxson, P., Mallicoat, S.W., Lukey, G.C., Kriven, W.M., Van Deventer, J.S.J.: The effect of alkali and Si/Al ratio on the development of mechanical properties of metakaolin-based geopolymers, *Colloid Surface A*, **292**, 8–20, (2007).
  - 18 Vidal, L., Joussein, E., Colas, M., Cornette, J., Sanz, J., Sobrados, I., Gelet, J.-L., Absi, J., Rossignol, S.: Controlling the reactivity of silicate solutions: A FTIR, raman and NMR study, *Colloid Surface A*, **503**, 101–109, (2016).
  - 19 Brewer, C.E., Chuang, V.J., Masiello, C.A., Gonnermann, H., Gao, X., Dugan, B., Driver, L.E., Panzacchi, P., Zygourakis, K., Davies, C.A.: New approaches to measuring biochar density and porosity, *Biomass Bioenerg.*, **66**, 176–185, (2014).
  - 20 Rafiq, M.K., Bachmann, R.T., Rafiq, M.T., Shang, Z., Joseph, S., Long, R.: Influence of pyrolysis temperature on physico-chemical properties of corn stover (*Zea mays* L.) biochar and feasibility for carbon capture and energy balance, *Plos One*, **11**, 6, (2016).
  - 21 Gray, M., Johnson, M.G., Dragila, M.I., Kleber, M.: Water uptake in biochars: the roles of porosity and hydrophobicity, *Biomass Bioenerg.*, **61**, 196–205, (2014).
  - 22 Werner, K., Pommer, L., Broström, M.: Thermal decomposition of hemicelluloses, *J. Anal. Appl. Pyrol.*, **110**, 130–137, (2014).
  - 23 Yang, H., Yan, R., Chen, H., Lee, D.H., Zheng, C.: Characteristics of hemicellulose, cellulose and lignin pyrolysis, *Fuel*, **86**, 1781–1788, (2007).
  - 24 Wang, S., Dai, G., Yang, H., Luo, Z.: Lignocellulosic biomass pyrolysis mechanism: A state-of-the-art review, *Prog. Energ. Combust.*, **62**, 33–86, (2017).
  - 25 Sarmah, A.K., Srinivasan, P., Smernik, R.J., Manley-Harris, M., Antal, M.J., Downie, A., Van Zwieten, L.: Retention capacity of biochar-amended new zealand dairy farm soil for an estrogenic steroid hormone and its primary metabolite, *Soil Res.*, **48**, 648–658, (2010).
  - 26 Stuart, B.H.: Infrared spectroscopy: Fundamentals and applications. Ed. John Wiley & Sons, Chichester (UK), 2004.
  - 27 Lou, K., Rajapaksha, A.U., Ok, Y.S., Chang, S.X.: Pyrolysis temperature and steam activation effects on sorption of phosphate on pine sawdust biochars in aqueous solutions, *Chem. Spec. Bioavailab.*, **28**, 42–50, (2016).
  - 28 Bahng, M.-K., Donohoe, B.S., Nimlos, M.R.: Application of a fourier transform-infrared imaging tool for measuring temperature or reaction profiles in pyrolyzed wood, *Energ Fuel*, **25**, 370–378, (2011).
  - 29 Haberhauer, G., Rafferty, B., Strebl, F., Gerzabek, M.H.: Comparison of the composition of forest soil litter derived from three different sites at various decompositional stages using FTIR spectroscopy, *Geoderma*, **83**, 331–342, (1998).
  - 30 Smidt, E., Meissl, K.: The applicability of fourier transform infrared (FT-IR) spectroscopy in waste management, *Waste Manage.*, **27**, 268–276, (2007).
  - 31 Huang, C.K., Kerr P.F.: Infrared study of the carbonate minerals, *Am Mineral.*, **45**, [3–4], 311–24, (1960).
  - 32 Socrates, G.: Infrared and raman characteristic group frequencies: Tables and charts. John Wiley and Sons, Chichester (UK), 2000.
  - 33 Lu, P., Hsieh, Y.-L.: Highly pure amorphous silica nano-disks from rice straw, *Powder Technol.*, **225**, 149–155, (2012).
  - 34 Qian, L., Chen, B.: Dual role of biochars as adsorbents for aluminum: the effects of oxygen-containing organic components and the scattering of silicate particles, *Environ. Sci. Technol.*, **47**, [15], 8759–8768, (2013).
  - 35 Periasamy, A., Muruganand, S., Palaniswamy, M.: Vibrational studies of Na<sub>2</sub>SO<sub>4</sub>, K<sub>2</sub>SO<sub>4</sub>, NaHSO<sub>4</sub> and KHSO<sub>4</sub> crystals, *Rasayan J. Chem.*, **2**, [4], 981–989, (2009).
  - 36 El Khouri, A., Elahtmani, M., Della Ventura, G., Sodo, A., Rizzi, R., Rossi, M., Capitelli, F.: Synthesis, structure refinement and vibrational spectroscopy of new rare-earth tricalcium phosphates Ca<sub>9</sub>RE(PO<sub>4</sub>)<sub>7</sub> (RE = La, Pr, Nd, Eu, Gd, Dy, Tm, Yb), *Ceram Int.*, **43**, 15645–15653, (2017).
  - 37 Duxson, P., Lukey, G.C., van Deventer, J.S.J.: Thermal conductivity of metakaolin geopolymers used as a first approximation for determining gel interconnectivity, *Ind. Eng. Chem. Res.*, **45**, [23], 7781–7788, (2006).